Nam *et al. Nano Convergence* (2019) 6:40
https://doi.org/10.1186/s40580-019-0205-2

Nano Convergence

RESEARCH Open Access

NO_2 sensing properties of WO_3-decorated In_2O_3 nanorods and In_2O_3-decorated WO_3 nanorods

Bumhee Nam, Tae-Kyoung Ko, Soong-Keun Hyun* and Chongmu Lee*

Abstract

In_2O_3 nanoparticle (NP)-decorated WO_3 nanorods (NRs) were prepared using sol–gel and hydrothermal methods. The In_2O_3 NRs and WO_3 NPs were crystalline. WO_3 NP-decorated In_2O_3 NRs were also prepared using thermal evaporation and hydrothermal methods. The NO_2 sensing performance of the In_2O_3 NP-decorated WO_3 NR sensor toward NO_2 was compared to that of the WO_3 NP-decorated In_2O_3 NR sensor. The former showed a high response to NO_2 due to a significant reduction of the conduction channel width upon exposure to NO_2. In contrast, the latter showed a far less pronounced response due to limited reduction of the conduction channel width upon exposure to NO_2. When the sensors were exposed to a reducing gas instead of an oxidizing gas (NO_2), the situation was reversed, i.e., the WO_3 NP-decorated In_2O_3 NR exhibited a stronger response to the reducing gas than the In_2O_3 NP-decorated WO_3 NR sensor. Thus, a semiconducting metal oxide (SMO) with a smaller work function must be used as the decorating material in decorated heterostructured SMO sensors for detection of oxidizing gases. The In_2O_3 NP-decorated WO_3 NR sensor showed higher selectivity for NO_2 compared to other gases, including reducing gases and other oxidizing gases, as well as showed high sensitivity to NO_2.

Keywords: Gas sensor, Heterostructure, WO_3, In_2O_3, NO_2

1 Introduction

Despite the numerous merits of semiconducting metal oxides (SMOs) as sensor materials there are still certain limitations, such as their relatively low response to gases at room temperature and dissatisfactory selectivity [1]. To address the dissatisfactory sensing properties, various strategies have been attempted, including noble metal catalyst doping, heterojunction formation, and radiation-assisted treatment with energetic particles including ion beams, electrons, and ultraviolet (UV) lights [2–4]. Of these techniques, heterostructure formation is plausibly most widely studied and is used for the fabrication of chemiresistive nanostructured gas sensors. There are several types of heterostructures including p-n, n–n and p–p heterostructures. Generally, p–p heterostructures are less commonly utilized because of their inferior sensing properties, whereas n–n heterostructures are as widely utilized as the p–n counterparts because of their superior sensing properties [5]. However, strangely, n–n heterostructures have not been studied as intensively as the p–n congeners. The enhanced sensing properties of n–n heterostructures are mainly due to the resistance modulation at the n–n heterojunctions in n–n heterostructures. Various heterostructure combinations are known, such as a simple mixture of two different types of n-SMOs [6], bi-layer type n–n nanostructures [7], n–n core–shell structures [8], a single type of n-SMO nanostructure decorated with another type of n-SMO nanoparticles (NPs) [9], etc.

This study focuses on, decorated n–n heterostructures. WO_3 and In_2O_3 are chosen as sensor materials for detecting a typical oxidizing gas, NO_2. The sensing properties

*Correspondence: skhyun@inha.ac.kr; cmlee@inha.ac.kr
Department of Materials Science and Engineering, Inha University, 253 Yonghyun-dong, Nam-gu, Incheon 402-751, Republic of Korea

Springer Open

© The Author(s) 2019. This article is distributed under the terms of the Creative Commons Attribution 4.0 International License (http://creativecommons.org/licenses/by/4.0/), which permits unrestricted use, distribution, and reproduction in any medium, provided you give appropriate credit to the original author(s) and the source, provide a link to the Creative Commons license, and indicate if changes were made.

of In_2O_3 NP-decorated WO_3 nanorods (NRs), WO_3 NP-decorated In_2O_3 NRs, pristine WO_3 NRs, and pristine In_2O_3 NRs are compared and the differences in the sensing properties of these four nanostructures are analyzed and the origin of the differences is discussed in detail.

2 Methods

2.1 Preparation of In_2O_3 nanoparticles-decorated WO_3 nanorods

High purity In_2O_3 NPs were synthesized using a sol–gel method [10]. Indium acetate ($[In(C_2H_3O_2)2{\cdot}H_2O]$; 0.6695 g) was dissolved in diethylene glycol and stirred for 5 min. The solution was homogenized by heating to 130 °C and 3 mL of 3 *N*-nitric acid was added to the solution and stirred well. The solution was heated at 180 °C for 5 h, and pure yellowish In_2O_3 NPs were precipitated. The In_2O_3 NPs were dried at 400 °C for 2 h and then calcined at 500 °C for 1 h to obtain the pure In_2O_3 NPs. The WO_3 NRs were synthesized by using a low-temperature hydrothermal method [11]. Sodium tungstate (1.956 mL) and oxalic acid (1.512 mL) were dissolved in distilled water (50 mL). The solution was acidified to PH 0.7–0.9 by mixing with 3 mol/L HCl solution. A transparent precursor solution was formed and 3 g of K_2SO_4 was added to the solution. The mixed solution was maintained in an autoclave at 100 °C for 24 h, cooled to room temperature, and was centrifuged to collect the green product. The product was rinsed with ethanol and dried at 60 °C for 1 h to obtain pure WO_3 NRs. The substrate on which the WO_3 NRs were synthesized was placed on a spin coater and then rotated at 500 rpm. The In_2O_3 NPs synthesized via the sol–gel method were dispersed in ethanol with a micropipette and the ethanolic dispersion of In_2O_3 NPs was dropped on the rotating WO_3 NR substrate.

2.2 Preparation of WO_3 nanoparticles-decorated In_2O_3 nanorods

In_2O_3 NRs were synthesized using a thermal evaporation method [12]. A 3 mm thick gold film—coated p-type Si (100) substrate was placed on the top of an alumina boat containing a mixture of In_2O_3 powders and positioned at the center of a horizontal quartz tube furnace. The furnace was heated to 900 °C and maintained at that temperature for 30 min under argon gas at a constant flow rate of 200 cm^3/min. The WO_3 NPs were synthesized using a hydrothermal method [13]. WO_3 powders (2 mL) were dissolved in 48 mL of hydrochloric acid in sonicater. The pH of the solution was controlled at 7 using sodium hydroxide. After sonication of the solution for 6 h the precipitated powders were collected by removing the liquid, leaving the powders behind. The powders were placed into a hydrothermal synthesizer containing ethanol and the synthesizer was placed in an oven and heated at 180 °C for 12 h. WO_3 NPs were synthesized in the hydrothermal synthesizer. The substrate on which the In_2O_3 NRs were synthesized by the thermal evaporation method was placed in a beaker containing ethanol and then ultrasonicated to separate the In_2O_3 NRs from the substrate. Meanwhile, the WO_3 NPs synthesized by the hydrothermal method were dispersed in ethanol. The two solutions (In_2O_3 NRs dispersed in ethanol and the WO_3 NPs dispersed in ethanol) were mixed and the mixed solution was exposed to UV (254 nm) irradiation for 12 h using a UV lamp. The mixed solution was then annealed under argon atmosphere at 400 °C for 1 h in an annealing furnace.

2.3 Fabrication of chemiresistive sensors

The In_2O_3 NP-decorated WO_3 NRs and WO_3 NP-decorated In_2O_3 NRs grown on the Si substrate were dispersed ultrasonically in isopropyl alcohol. A multiple-networked chemiresistive sensor was fabricated by pouring the solution containing the precursors of the two different nanostructures onto SiO_2/Si substrates with a patterned interdigital electrode with a double layer comprising separate layers of Ti (10 nm) and Au (100 nm): the assembly was dried at 150 °C for 1 min. For comparison of the sensing properties, pristine In_2O_3 and WO_3 NR sensors were also fabricated in a similar manner.

2.4 Characterization

The microstructures and phases of the synthesized NR samples were examined by scanning electron microscopy (SEM) and X-ray diffraction (XRD), respectively. The microstructures and phases of the samples were examined further by transmission electron microscopy (TEM).

2.5 Gas sensing tests

The NO_2 sensing performances of the fabricated sensors were examined using a custom-made gas sensing system. The concentration of NO_2 gas was controlled precisely in the concentration range of 5–200 ppm by mixing NO_2 with dry synthetic air using the mass flow controllers. Electrical measurements to examine the sensing properties of the sensors were conducted at room temperature under 50% relative humidity. The detailed sensing test procedure is described elsewhere [14]. The response of the sensors to NO_2 was evaluated by using the R_g/R_a ratio, where R_g and R_a are the resistances of the sensor measured in the presence of air and NO_2, respectively. The response and recovery times were determined by measuring the times required to reach 90% of the total

change in the resistance of the sensor after exposure of the sensor to the analyte gas and ambient air, respectively.

3 Results and discussion

Figure 1a, b show low-magnification TEM images of the pristine and In_2O_3 NPs-decorated WO_3 NRs, respectively. The average diameter of the WO_3 NRs was ~ 50 nm and the length of the WO_3 NRs ranged from 200 to 1100 nm. The average diameter of the In_2O_3 NPs on the WO_3 NRs was 20 nm. The SEM images of the pristine and WO_3 NP-decorated In_2O_3 NRs are exhibited in Fig. 1c, d. The average diameter of the In_2O_3 NRs was 250 nm and the lengths of the In_2O_3 NRs ranged from 1 to 10 μm. The average diameter of the WO_3 NPs on the In_2O_3 NRs was 140 nm. Hence, the average diameter of the WO_3 NPs on the In_2O_3 NRs was ~ 7 times larger than that of the In_2O_3 NPs on the WO_3 NRs. The difference in size might be due to the different preparation methods (sol–gel versus hydrothermal methods).

Figure 2a, b show the XRD patterns of the In_2O_3 NP-decorated WO_3 NRs and WO_3 NP-decorated In_2O_3 NRs, respectively. In the former pattern, the WO_3 NRs exhibited relatively sharp and intense reflection peaks, assigned to the primitive tetragonal structured WO_3 (JCPDS card No. 89-4481, a = 0.5275 nm, c = 0.7846 nm). In contrast, the In_2O_3 NPs exhibited relatively less sharp and less intense reflection peaks, assigned to body-centered cubic In_2O_3 with a lattice constant of $a = 1.011$ nm (JCPDS No. 89-4595). The lower intensity peaks for In_2O_3 compared to WO_3 might be due to the smaller volume of the In_2O_3 NPs relative to that of the WO_3 NRs. In contrast, in the latter pattern (Fig. 2b), In_2O_3 peaks were

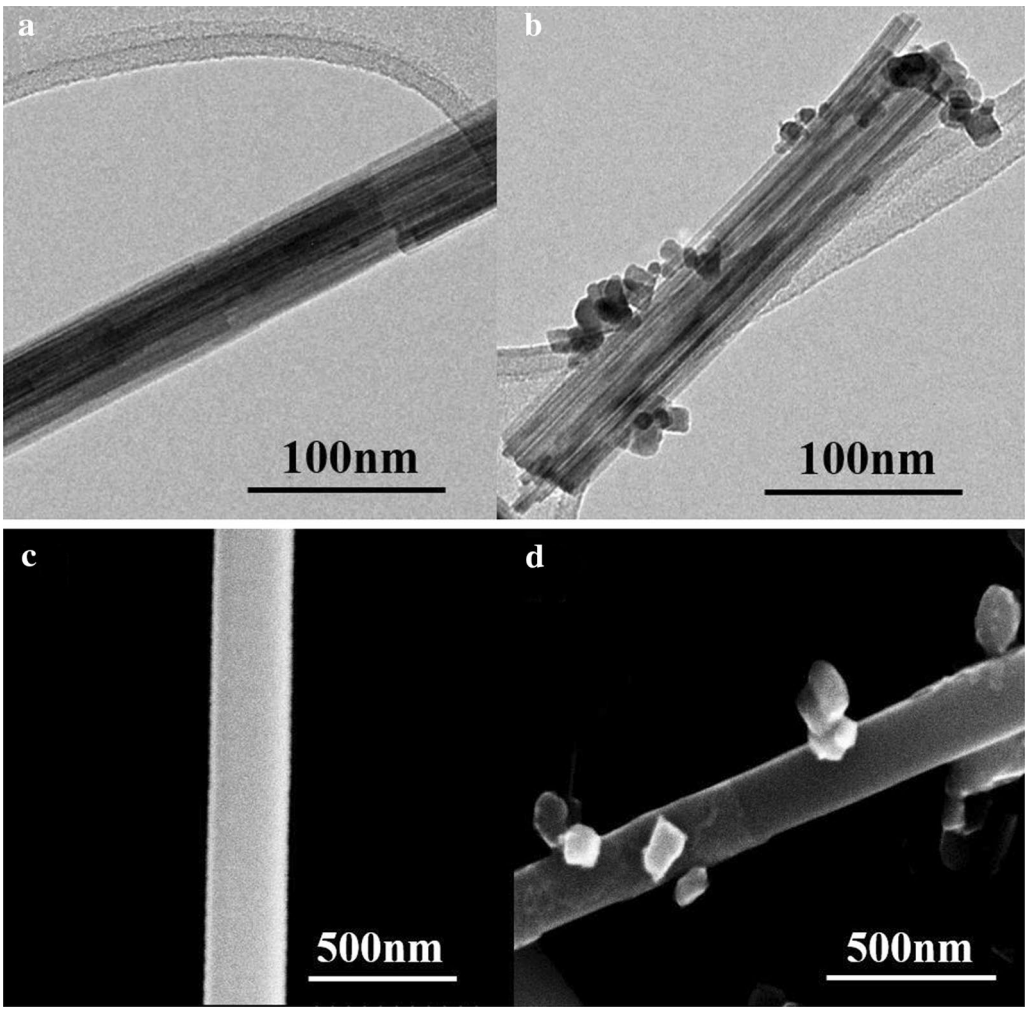

Fig. 1 Low-magnification TEM images: **a** pristine and **b** In_2O_3 NPs-decorated WO_3 NRs and SEM images: **c** pristine and **d** WO_3 NPs-decorated In_2O_3 NRs

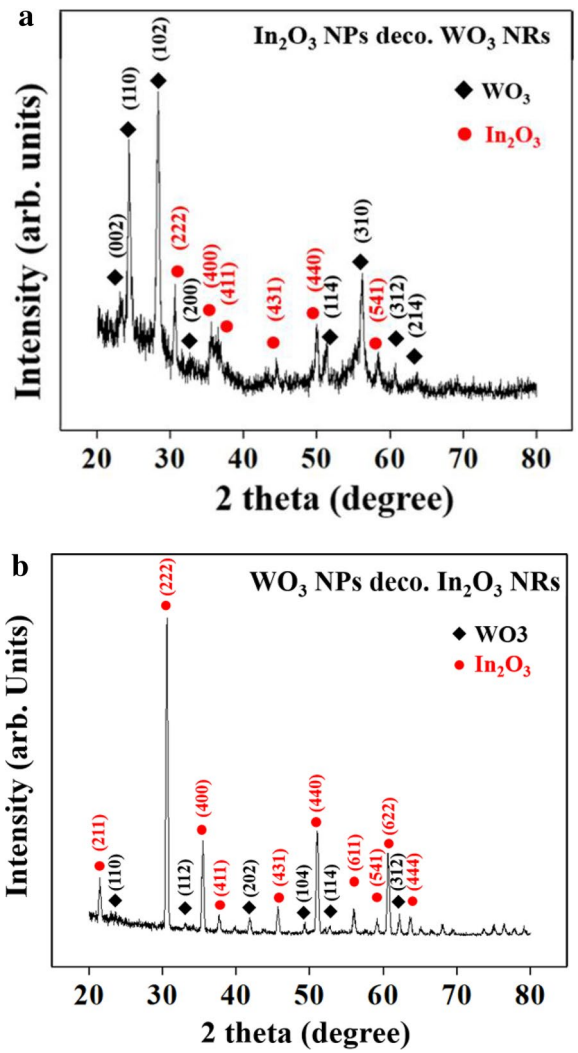

Fig. 2 XRD patterns of **a** In_2O_3 NPs-decorated WO_3 NRs and **b** WO_3 NPs-decorated In_2O_3 NRs

taller and sharper than WO_3 peaks, which might be due to the larger volume of In_2O_3 NRs than those of the WO_3 NPs.

Figure 3a, b present the high-resolution TEM image and corresponding selected area electron diffraction (SAED) pattern of the In_2O_3 NP-decorated WO_3 NRs. The regularly aligned fringes in both the WO_3 and In_2O_3 regions suggest that the WO_3 and In_2O_3 nanostructures are both crystalline. The corresponding spotty electron diffraction (ED) pattern in Fig. 3b reveals that the WO_3 and In_2O_3 nanostructures are single crystals.

The temperature-dependent responses of all four different sensor materials to NO_2 are presented in Fig. 4. The responses of all the four sensor materials to NO_2 tended to increase with increasing temperature up to 300 °C, and then to decrease with further increases in the temperature. This result suggests that 300 °C is the optimal operating temperature of the sensors in detecting the NO_2. All the sensing tests hereafter were conducted at 300 °C. At too low operating temperature (250 °C or lower), the NO_2 molecules may not have enough energy to overcome the energy barrier of adsorption, and fail to be adsorbed on the surface of the sensor materials, WO_3 and In_2O_3. However, at too high operating temperature (350 °C or higher), adsorption failure might also occur because the rate of desorption may outweigh that of adsorption [15].

Figure 5a–d present the dynamic response curves of the four different sensors toward NO_2. All the sensors showed stable and reversible response and recovery behavior. The resistances of the sensors increased when an oxidizing gas (NO_2) was supplied, and recovered to the initial value when the NO_2 supply was stopped and the sensors were exposed to ambient air. This response toward the oxidizing gas is in accord with the sensing behavior of n-type semiconductors. As is well known, both WO_3 and In_2O_3 are n-type semiconductors. The resistance changes increased as the NO_2 concentration was increased. The starting resistances of the pristine and WO_3 NP-decorated In_2O_3 NRs was markedly lower than the pristine and In_2O_3 NPs-decorated WO_3 NRs, respectively, which might be due to the much lower resistivity of In_2O_3 than that of WO_3.

Figure 6 shows the responses of the four different sensors to NO_2 as a function of the NO_2 concentration. The response of the In_2O_3 NP-decorated WO_3 NRs to NO_2 far exceeded those of the other three sensors over the entire NO_2 concentration range. The more pronounced response of the In_2O_3 NP-decorated WO_3 NR sensor to NO_2 than that of the pristine WO_3 NRs and the greater response of the WO_3 NPs-decorated In_2O_3 NRs sensor to NO_2 than that of the pristine In_2O_3 NRs is plausibly due to the resistance modulation at the WO_3–In_2O_3 heterojunction formation [16]. Contrarily, the much stronger response of the In_2O_3 NP-decorated WO_3 NR sensor to NO_2 than that of the WO_3 NP-decorated In_2O_3 NR sensor is very interesting. The origin of this difference in the response of the heterostructured sensors with inverse configuration is discussed in detail in the next section.

Figure 7a, b show the response and recovery times of the four different sensors toward NO_2 as a function of the NO_2 concentration. As expected, the response and recovery times of the In_2O_3 NP-decorated WO_3 NR sensor were shorter than those of the pristine WO_3 NRs. In contrast, the response and recovery times of the WO_3 NP-decorated In_2O_3 NR sensor were longer than those of the pristine In_2O_3 NR sensor. Comparison of the response

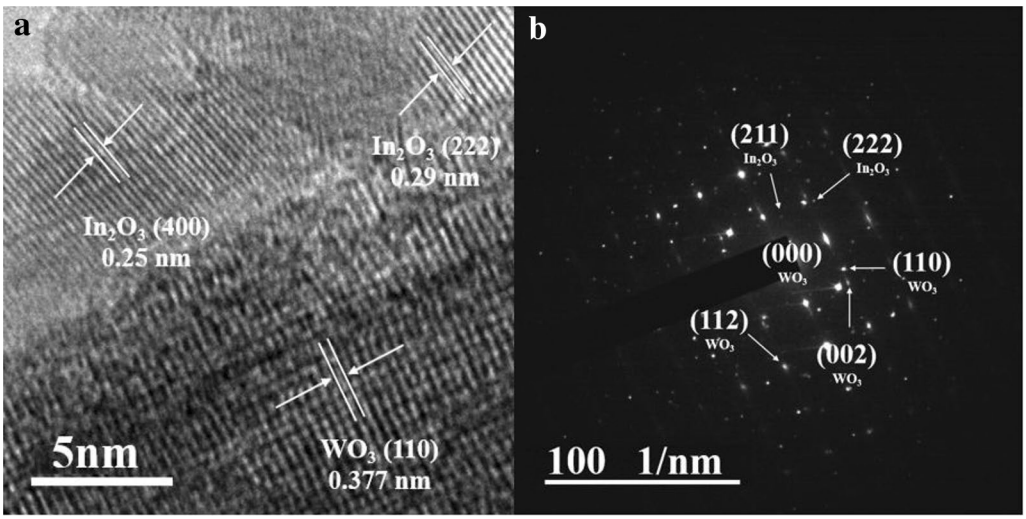

Fig. 3 **a** High-resolution TEM image, **b** corresponding electron diffraction pattern of the In_2O_3 NPs-decorated WO_3 NRs

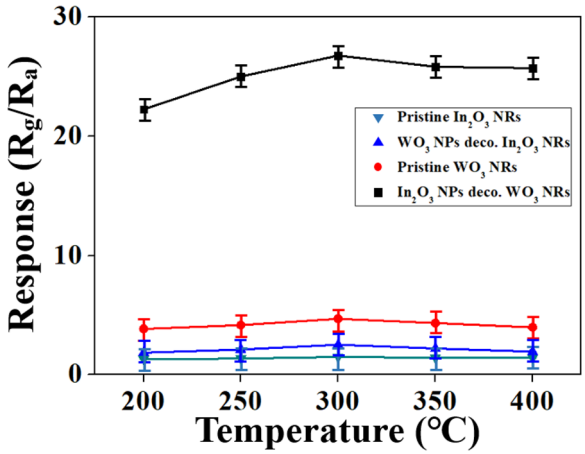

Fig. 4 Responses of In_2O_3 NPs-decorated WO_3 NRs and WO_3 NPs-decorated In_2O_3 NPs along with pristine WO_3 NRs and pristine WO_3 NRs at various operating temperatures to NO_2

and recovery times of the In_2O_3 NP-decorated WO_3 NR sensor with those of the WO_3 NP-decorated In_2O_3 NR sensor, interestingly, shows shorter response and recovery times for the former in the higher NO_2 concentration range, whereas longer response and recovery times for the lower NO_2 concentration range than the latter. Shorter response and recovery times are commonly associated with a higher response for gas sensors.

The response of the In_2O_3 NP-decorated WO_3 NR sensor to various gases is shown in Fig. 8. The sensor showed a much stronger response to NO_2 than to the other oxidizing gases such as O_3 and SO_2 or reducing gases such as CO, CH_4 and H_2S, demonstrating the selectivity and sensitivity of the In_2O_3 NP-decorated WO_3 NR sensor toward NO_2. The selectivity of the sensor toward NO_2 against other gases might be related to the different optimal operating temperatures of the sensor for different target gases. The response of a sensor material to a certain gas might depend on many factors such as solid solubility of the gas in the material, the decomposition rate of the adsorbed molecule at the material surface, the charge carrier concentration in the material, the Debye length in the material, the catalytic activity of the material, the orbital energy of the gas molecule, etc. The dissociation (or reduction) rate of an oxidizing gas such as NO_2 is determined by these factors. Therefore, each gas has the characteristic optimal dissociation temperature at which its dissociation rate is maximized. The In_2O_3-decorated WO_3 nanorod sensor fabricated in this study showed higher response fortunately to NO_2 than other gases at 300 °C because of the higher dissociation rate of NO_2 at the surface of In_2O_3 and WO_3 at the temperature, but it might show higher responses to other gases than NO_2 at different temperatures [17–22].

Figure 9a–d illustrate the sensing mechanism of the In_2O_3 NP-decorated WO_3 NR sensor toward NO_2. Earlier studies reported that the response of a base sensor material could be enhanced by decoration with another type of SMO NPs, mainly because of the greater modulation of the width of the depletion layer or the conduction channel, resulting in the greater modulation of the sensor resistance [23–25]. n-Type WO_3 has a larger work function ($q\Phi$) than n-type In_2O_3 (Fig. 9a). Accordingly, if WO_3 and In_2O_3 are in contact, even under vacuum, electron transfer from In_2O_3 (with a larger work function) to WO_3 (with a smaller work function) tends to

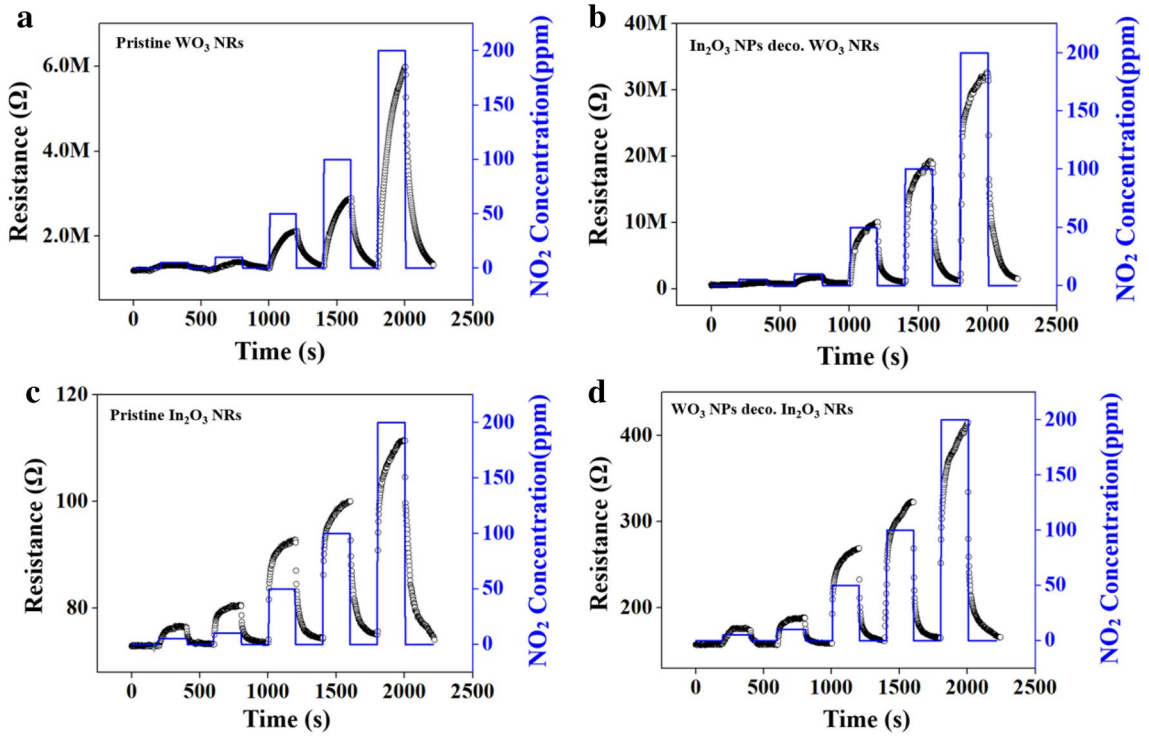

Fig. 5 Dynamic response curves: **a** pristine WO_3 NRs to NO_2, **b** In_2O_3 NPs-decorated WO_3 NRs to NO_2, **c** pristine In_2O_3 NRs to NO_2, and **d** WO_3 NPs-decorated In_2O_3 NRs to NO_2

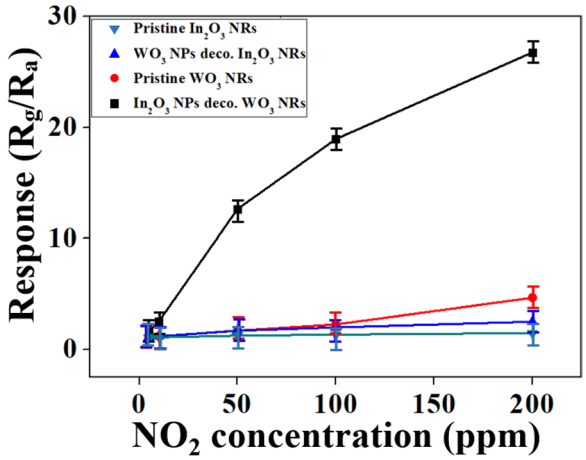

Fig. 6 Calibration curves for responses of pristine and In_2O_3 NPs-decorated WO_3 to NO_2 as well as those of pristine and WO_3 NPs-decorated In_2O_3 NRs to NO_2 as a function of NO_2 concentrations

occur until electronic equilibrium is attained between WO_3 and In_2O_3, as shown in Fig. 9a. Consequently, electron-accumulation and electron-depletion layers are formed in the WO_3 and In_2O_3 regions, respectively. The schematic shows the In_2O_3 NP-decorated WO_3 NRs with an accumulation layer with a width of W_{11}, formed by electron transfer from the In_2O_3 NPs to the WO_3 NRs (Fig. 9b). In ambient air, the surfaces of the WO_3 NR and In_2O_3 NP adsorb oxygen molecules and the adsorbed oxygen molecules are ionized by the capture of the free electrons in the WO_3 and In_2O_3 surface regions (Fig. 9c). Consequently, a depletion layer with a width of W_{12} is formed in the surface region of WO_3. The schematic shows a decorated WO_3 NR with a depletion layer formed via ionization of adsorbed oxygen molecules and an accumulation layer formed by electron transfer from the In_2O_3 to the WO_3 (Fig. 9c). When NO_2 gas is supplied, NO_2 and O_2 molecules are both adsorbed by the In_2O_3 and WO_3 surfaces. The adsorbed NO_2 molecules are converted into NO_2^- or NO [26, 27] and the adsorbed oxygen molecules are converted into oxygen ions by capturing electrons from the WO_3 and In_2O_3 surface regions. Consequently, a thicker depletion layer (with a width of W_{22}) (Fig. 9d) is formed than that formed in ambient air. The schematic shows a WO_3 NR with a depletion layer with a width of W_{22} as well as the accumulation layer with a width of W_{21} formed by the electron transfer from the In_2O_3 to the WO_3 (Fig. 9d).

The sensing mechanism of the WO_3 NP-decorated In_2O_3 NR sensor toward NO_2 is illustrated in Fig. 9e, f.

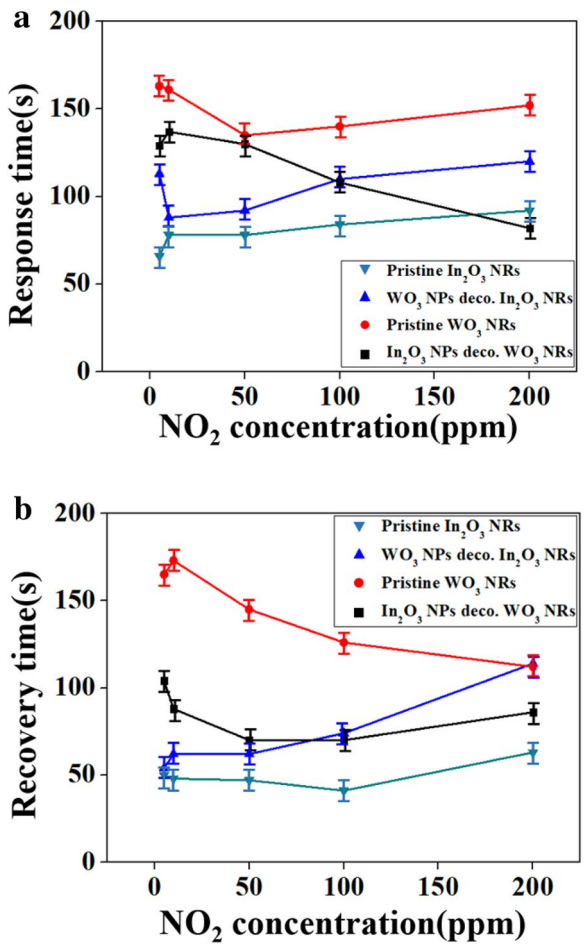

Fig. 7 Calibration curves for **a** response times and **b** recovery times of pristine and In_2O_3 NPs-decorated WO_3 NRs as well as pristine and WO_3 NPs-decorated In_2O_3 NRs to NO_2 as a function of NO_2 concentrations

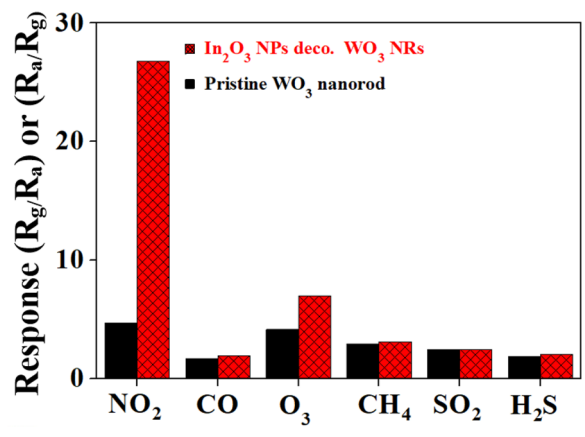

Fig. 8 Selectivity patterns of pristine and In_2O_3 NPs-decorated WO_3 NRs toward NO_2 against other gases such as O_3, SO_2, CO, CH_4, and H_2S

As discussed above, electron-accumulation and depletion layers are formed in the WO_3 and In_2O_3 regions, respectively. Thus, a depletion layer with a width of W_{31} forms on the In_2O_3 side of the WO_3–In_2O_3 interface (Fig. 9e). In ambient air, oxygen molecules are adsorbed by the In_2O_3 NR surface and ionized by accepting the electrons from the In_2O_3 and WO_3 surface regions. Consequently, a depletion layer with a width of W_{32} is formed in the In_2O_3 surface region. A WO_3 NP-decorated In_2O_3 NR with a depletion layer formed due to the ionization of adsorbed oxygen molecules and a depletion layer formed by electron transfer from the WO_3 NP is shown in Fig. 9e. Under NO_2 atmosphere, a thicker depletion layer (with a width of W_{42}) than that generated in ambient air is formed due to the adsorption and ionization of both NO_2 and O_2 molecules (Fig. 9f). Note that no electron-accumulation layer is formed in the In_2O_3 NR throughout the on–off cycling of the NO_2 gas supply.

Under ambient air and NO_2, there was no big difference in the basic response of the In_2O_3 NPs-decorated WO_3 NRs versus that of the WO_3 NPs-decorated In_2O_3 NRs. A relatively thin depletion layer is formed in both samples upon exposure to air and a thick depletion layer is generated upon exposure to NO_2. Consequently, the width of the conduction channel of the In_2O_3 NP-decorated WO_3 NRs formed upon exposure to NO_2 is much smaller than that of the WO_3 NP-decorated In_2O_3 NRs formed in ambient air. The conduction channel of the In_2O_3 NP-decorated WO_3 NRs has a room for substantial reduction upon exposure to NO_2 because the conduction channel width has already been expanded due to the formation of an accumulation layer by the transfer of electrons from the In_2O_3 NP to the WO_3 NR. In contrast, the conduction channel of the WO_3 NPs-decorated In_2O_3 NRs was already shrunken due to the formation of the electron-depletion layer via electron transfer from the In_2O_3 NR to the WO_3 NP. Accordingly, the conduction channel of the In_2O_3 NR has little room for further reduction upon exposure to NO_2 [28].

The response, S is defined as R_g/R_a. for the oxidizing gas NO_2 and S is proportional to A_a/A_g because the resistance $R = \rho l/A$, where ρ, l and A are the density, length and cross-sectional area of the conductor (channel, here) [29]. S can be expressed as the ratio of the conduction channel width for an analyte gas to that for air, $S = W_a^2/W_g^2$ because $A = \pi W^2$, where W is the conduction channel width. Therefore, the In_2O_3 NP-decorated WO_3 NR sensor has a higher response, S to NO_2 because of the far smaller conduction channel width, W_g in NO_2 atmosphere. In contrast, the WO_3 NP-decorated In_2O_3 NR sensor has a lower response, S because

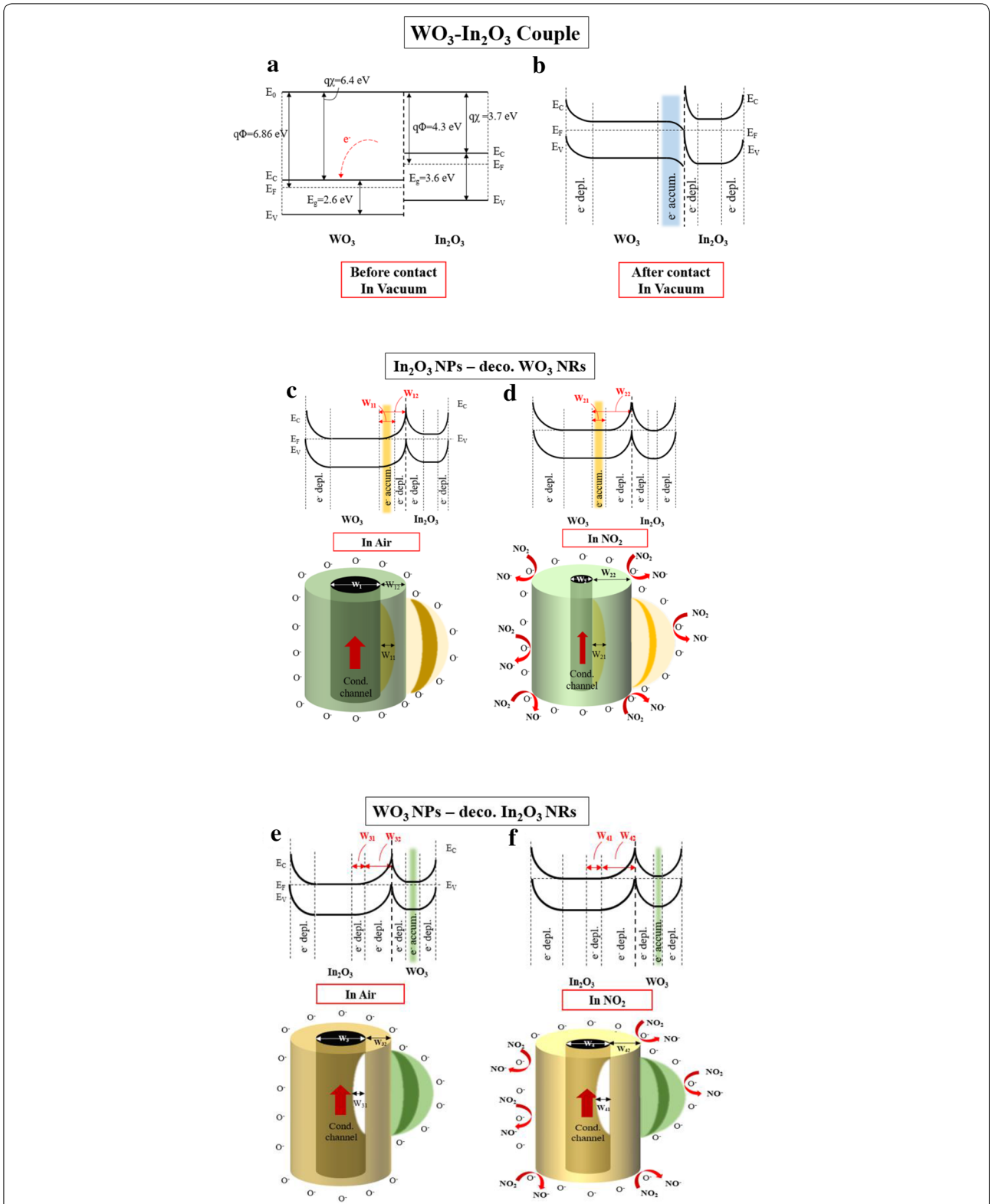

Fig. 9 Energy band diagrams of a WO_3-In_2O_3 couple **a** before and **b** after contact. Energy band diagrams and schematics of In_2O_3 NPs-decorated WO_3 NRs: **c** in air and **d** in NO_2, and of WO_3 NPs-decorated In_2O_3 NRs: **e** in air and **f** in NO_2

of the lower contraction of the conduction channel width, W_g in NO_2 atmosphere.

4 Conclusions

The sensing properties of the In_2O_3 NP-decorated WO_3 NR sensor toward NO_2 were compared to those of the WO_3 NP-decorated In_2O_3 NR sensor. The response of the former sensor to NO_2 was more pronounced than that of the latter due to the significant reduction of the conduction channel width of the former sensor upon exposure to NO_2. The conduction channel of the In_2O_3 NP-decorated WO_3 NR sensor had room for sufficient reduction as it was already expanded by electron transfer from the In_2O_3 NPs to the WO_3 NRs. In contrast, the WO_3 NP-decorated In_2O_3 NR sensor showed a lower response due to insufficient reduction of the conduction channel width upon exposure to NO_2. The conduction channel of the WO_3 NP-decorated In_2O_3 NR sensor had little room for further reduction due to prior shrinkage associated with electron transfer from the In_2O_3 NRs to the WO_3 NPs. For the detection of a reducing gas instead of an oxidizing gas, the magnitude of the sensor response would be reversed. Therefore, choosing a proper decorating material in fabricating n-SMO NR sensors decorated with n-SMO NPs is important in obtaining high sensitivity. An SMO with a smaller work function must be chosen as a decorating material in a decorated heterostructured sensor for oxidizing gas detection. In contrast, an SMO with a larger work function must be chosen as the decorating material for heterostructured sensors geared toward the detection of a reducing gas.

Abbreviations

NP: nanoparticle; NR: Nanorod; SMO: semiconducting metal oxide; UV: ultra violet; JCPDS: Joint Committee on Powder Diffraction Standards.

Acknowledgements

This work was supported by the National Research Foundation of Korea grant funded by the Korea government (MSIT), South Korea (No. 2017R1A2B4010034) and Basic Science Research Program through the National Research Foundation of Korea (NRF) funded by the Ministry of Education, South Korea (No.2016R1A6A3A11934765).

Authors' contributions

CML and SKH designed all major experiments. BHN and TGK performed all major experiments. CML wrote the manuscript. All authors read and approved the final manuscript.

Funding

This work was supported by the National Research Foundation of Korea grant funded by the Korea government (MSIT), South Korea (No. 2017R1A2B4010034) and Basic Science Research Program through the National Research Foundation of Korea (NRF) funded by the Ministry of Education, South Korea (No. 2016R1A6A3A11934765).

Availability of data and materials

The datasets used and/or analyzed during the current study are available from the corresponding author on reasonable request.

Competing interests

The authors declare that they have no competing interests.

Received: 22 July 2019 Accepted: 4 October 2019
Published online: 13 December 2019

References

1. A.C. Romain, J. Nicolas, Long term stability of metal oxide-based gas sensors for e-nose environmental applications: an overview. Sens. Actuators B Chem. **146**, 502–506 (2010)
2. G. Lu, L.E. Ocola, Room-temperature gas sensing based on electron transfer between discrete tin oxide nanocrystals and multiwalled carbon nanotubes. Adv. Mater. **21**, 2487 (2009)
3. D.R. Miller, S.A. Akbar, P.A. Morris, Nanoscale metal oxide-based heterojunctions for gas sensing: a review. Sens. Actuators B **204**, 250–272 (2014)
4. D.S. Dhawale, R.R. Salunkhe, V.J. Fulari, M.C. Rath, S.N. Sawant, C.D. Lokhande, Liquefied petroleum gas (LPG) sensing performance of electron beam irradiated chemically deposited TiO_2 thin films. Sens. Actuators B **141**, 58–64 (2009)
5. H.J. Kim, J.H. Lee, Highly sensitive and selective gas sensors using p-type semiconductors: Overview. Sens. Actuators B **192**, 607–627 (2014)
6. D. Shaposhnik, R. Pavelko, E. Llobet, F. Gispert-Guirado, X. Vilano, Hydrogen sensors on the basis of SnO_2–TiO_2 systems. Proc. Eng. **25**, 1133–1136 (2011)
7. R. Vasiliev, M. Rumyantseva, Effect of interdiffusion on electrical and gas sensor properties of CuO/SnO_2 heterostructure. Mater. Sci. **57**, 241–246 (1999)
8. S. Park, S. Kim, H. Kheel, C. Lee, Oxidizing gas sensing properties of the n-ZnO/p-Co_3O_4 composite nanoparticle network sensor. Sens. Actuators B Chem **222**, 1193–1200 (2015)
9. U. Shaislamov, B.L. Yang, CdS sensitized single-crystalline TiO_2 nanorods and polycrystalline nanotubes for solar hydrogen generation. J. Mater. Res. **28**, 418–423 (2012)
10. S. Elouali, L.G. Bloor, R. Binions, I.P. Parkin, C.J. Carmalt, J.A. Darr, Gas sensing with nano-indium oxides (In_2O_3) prepared via continuous hydrothermal flow synthesis. Langmuir **28**, 1879–1885 (2012)
11. Y. Yan, L. Chou, Competitive growth of In_2O_3 nanorods with rectangular cross sections. Appl. Phys. A **92**, 401–405 (2008)
12. J.K. Lee, W.S. Lee, W.I. Lee, S.B. Choi, S.K. Hyun, C.M. Lee, Selective detection of a reducing gas using WO_3-decorated ZnO nanorod-based sensor in the presence of oxidizing gases. Phys. Status Solidi A **215**, 1700929 (2018)
13. M. Shibuya, M. Miyauchi, Site-selective deposition of metal nanoparticles on aligned WO_3 nanotrees for super-hydrophilic thin films. Adv. Mater. **21**, 1373–1376 (2009)
14. S.H. Kim, S.H. Park, S.Y. Park, C.M. Lee, Acetone sensing of Au and Pd-decorated WO_3 nanorod sensors. Sens. Actuators B **209**, 180–185 (2015)
15. G.J. Sun, J.K. Lee, S.B. Choi, W.I. Lee, H.W. Kim, C.M. Lee, Selective oxidizing gas sensing and dominant sensing mechanism of n-CaO-Decorated n-ZnO nanorod sensors. ACS Appl. Mater. Interfaces. **9**, 9975–9985 (2017)
16. W. Wang, Z. Li, W. Zheng, H. Huang, C. Wang, J. Sun, Cr2O3-sensitized ZnO electrospun nanofibers based on ethanol detectors. sens. Actuators B **143**, 754–758 (2010)
17. J. Parrondo, R. Santhanam, F. Mijangos, B. Rambabu, Electrocatalytic performance of In_2O_3-supported Pt/C nanoparticles for ethanol electrooxidation in direct ethanol fuel cells. Int. J. Electrochem. Sci. **5**, 1342–1354 (2010)
18. K.I. Choi, H.R. Kim, K.M. Kim, D. Liu, G. Cao, J.H. Lee, C_2H_5OH sensing characteristics of various Co_3O_4 nanostructures prepared by solvothermal reaction. Sens. Actuators B: Chem. **146**, 183–189 (2010)
19. Y. Li, J. Xu, J. Chao, D. Chen, S. Ouyang, J. Ye, G. Shen, High-aspect-ratio single-crystalline porous In_2O_3 nanobelts with enhanced gas sensing properties. J. Mater. Chem. **21**, 12852–12857 (2011)
20. Z. Wen, L. Tianmo, Gas-sensing properties of SnO_2-TiO_2-based sensor for volatile organic compound gas and its sensing mechanism. Phys. B **405**, 1345–1348 (2010)
21. C. Feng, W. Li, C. Li, L. Zhu, H. Zhang, Y. Zhang, S. Ruan, W. Chen, L. Yu, Highly efficient rapid ethanol sensing based on $In_{2-x}Ni_xO_3$ nanofibers. Sens. Actuators B Chem. **166–167**, 83–88 (2012)

22. S. Park, S. Kim, G. Sun, C. Lee, Synthesis, structure, and ethanol gas sensing properties of In_2O_3 nanorods decorated with Bi_2O_3 nanoparticles. ACS Appl. Mater. Interfaces **7**, 8138–8146 (2015)
23. K. Vanheusden, W.L. Warren, C.H. Seager, D.R. Tallant, J.A. Voigt, B.E. Gnade, J. Appl. Phys. **79**, 7983–7990 (1996)
24. H.S. Woo, C.W. Na, I.D. Kim, J.H. Lee, Highly sensitive and selective trimethylamine sensor using one-dimensional ZnO–Cr_2O_3 heterostructures. Nanotechnology **23**, 24550123 (2012)
25. M. Mashock, K. Yu, S. Cui, S. Mao, G. Lu, J. Chen, Modulating gas sensing properties of CuO nanowires through creation of discete nanosized p–n junctions on their surfaces. ACS Appl. Mater. Interfaces **4**, 4192–4199 (2012)
26. T.V. Belysheva, L.P. Bogovtseva, E.A. Kazachkov, N.V. Serebryakova, Gas-sensing properties of doped In_2O_3 films as sensors for NO_2 in air. J. Anal. Chem. **58**, 583–587 (2003)
27. R. Ferro, J.A. Rodríguez, P. Bertrand, Peculiarities of nitrogen dioxide detection with sprayed undoped and indium-doped zinc oxide thin films. Thin Solid Films **516**, 2225–2230 (2008)
28. S.W. Choi, A. Katochi, J.H. Kim, S.S. Kim, Striking sensing improvement of n-type oxide nanowires by electronic sensitization based on work function difference. J. Mater. Chem. C **3**, 1521–1527 (2015)
29. E. S. Yang, Fundametals of Semiconductor Device (McGraw-Hill Inc., New York, 1978). ISBN 10: 0070722366 ISBN 13: 9780070722361

Publisher's Note

Springer Nature remains neutral with regard to jurisdictional claims in published maps and institutional affiliations.

Submit your manuscript to a SpringerOpen journal and benefit from:

- ► Convenient online submission
- ► Rigorous peer review
- ► Open access: articles freely available online
- ► High visibility within the field
- ► Retaining the copyright to your article

Submit your next manuscript at ► springeropen.com